JOURNAL OF AIRCRAFT
Vol. 40, No. 6, November–December 2003

Calculation of Rotor Blade–Vortex Interaction Airloads Using a Multiple-Trailer Free-Wake Model

Joon W. Lim* and Yung H. Yu†
U.S. Army Aviation and Missile Command, Moffett Field, California 94035
and
Wayne Johnson‡
NASA Ames Research Center, Moffett Field, California 94035

Analytical results of rotor blade–vortex interaction airloads are presented with two different wake models in the comprehensive analysis CAMRAD II, and these calculated results are compared with the experimental data obtained from the higher-harmonic-control aeroacoustic rotor test (HART-I) program. The HART rotor was a 40%, Mach-scaled model of the hingeless BO-105 main rotor. Two wake models used in the comprehensive analysis are the single-trailer and the multiple-trailer free-wake models. The multiple-trailer wake model shows good prediction of lift distribution, M^2c_n, as a function of azimuth for baseline, minimum noise, and minimum vibration cases, and shows significant improvement relative to the single-trailer model in prediction of the tip vortex wake geometry.

Nomenclature

c_n	=	blade section normal force coefficient
f_{cons}	=	fraction rollup
G	=	total strength of trailed vorticity
k_{cons}	=	consolidation scaling factor
M	=	Mach number
r	=	blade radial station
r_C	=	centroid of vorticity
r_G	=	moment (radius of gyration) of vorticity
α_S	=	rotor shaft angle (positive aft)
Γ	=	blade bound circulation
τ	=	wake age for the trailed vortex filament
τ_{cons}	=	consolidation time constant

Introduction

BLADE–VORTEX interactions (BVI) are the source of annoying and intrusive noise from helicopter rotors. This phenomenon is one of the distinctive features of rotor wakes, and the noise source becomes dominant during low-speed descent and maneuvering flights, where the rotor wake is blown back into the rotor plane. High noise levels produced by BVI may prevent rotorcraft from achieving wide acceptance for civil applications.

In the last decade, many investigations have been conducted to demonstrate the potentially high payoff in noise and vibration reduction using higher-harmonic blade pitch control (HHC) inputs. Although the HHC technique was originally intended for vibration reduction, several wind-tunnel and flight tests have shown BVI noise reduction of up to 10 dB with the application of HHC inputs, while vibration and low-frequency noise levels were increased.[1–5] However, with certain HHC schedules (amplitude and phase), simultaneous reduction of noise and vibration has been found to be achievable. Better physical understanding and analytical models are necessary to explain the basic physics of the noise and vibration reduction.

In 1994, researchers from DLR, German Aerospace Research Center, French ONERA, NASA Langley Research Center, the German–Netherlands Wind Tunnel (DNW), and the U.S. Army Aeroflightdynamics Directorate conducted the first higher-harmonic aeroacoustics rotor test (HART) rotor test with a 40% Mach-scaled model of a BO-105 main rotor in the open-jet anechoic test section of the DNW.[6–11] In this HART-I test, extensive measurements of acoustics, blade pressures, and blade deformations were made, as well as limited rotor wake measurements each at one azimuth angle on the advancing side and the retreating side. More detailed information about the measurements is available in Ref. 8.

Previous correlation efforts with the HART-I data,[12–15] revealed that accurate prediction of 2-per-revolution harmonic component of the lift distribution is a very challenging task. Some adjustments to comprehensive analysis models were necessary to achieve reasonable accuracy of the prediction, such as prescribing blade torsion from the measured data or vortex wake geometry iterative refinement.

The purpose of this paper is to explore a multiple-trailer free-wake model in CAMRAD II[16,17] for further improvement of the rotor airload prediction capability.

Experimental Data

Three HART-I cases selected for comparison with the experimental data were the baseline case [(BL) run 140], minimum noise case [(MN) run 138], and minimum vibration case [(MV) run 133]. These cases were for the same descent flight condition with an advance ratio of 0.15, a shaft angle of 5.3-deg aft (4.2-deg aft when adjusted for wind-tunnel correction), a hover tip Mach number of 0.64, and a thrust coefficient of 0.0044. The BL case is a normal descent flight condition without higher-harmonic pitch control inputs. The MN case has 3-per-revolution HHC inputs with 0.87-deg amplitude and 296-deg phase shift, which generates lower noise. The MV case has 3-per-revolution HHC inputs of 0.83-deg amplitude and 178-deg phase shift, which produces MV. More detailed information about the test data is available in Ref. 8.

CAMRAD II Rotor Modeling

The rotor blade experiences strong induced velocity fields due to the close passage of tip vortices, which have been trailed from the blade itself or the other blades. For very close interactions, viscous effects can be important, and transonic effects can be also important at high-speed flights. These effects could be modeled by the use of

Received 24 October 2002; revision received 15 April 2003; accepted for publication 16 April 2003.

*Aerospace Engineer, U.S. Army/NASA Rotorcraft Division, Aeroflightdynamics Directorate.
†Chief Scientist, U.S. Army/NASA Rotorcraft Division, Aeroflightdynamics Directorate.
‡Aeronautical Engineer, U.S. Army/NASA Rotorcraft Division.

sophisticated methods such as full-blown computational fluid dynamics (CFD) methods, but due to computational complexity and high computation time requirement, the usage of these methods has been limited for rotorcraft airloads calculation. Instead, the lift-line theory has been frequently used for general rotor application, accompanied with a complex rotor wake model and with various corrections to reflect complex physics of unsteady rotor aerodynamics, which has been typically a part of the comprehensive rotorcraft analysis.

For a rotor structure, the blade was structurally discretized into 16 nonlinear beam elements (finite element), with more beam elements aligned inboard to capture the blade structural behavior accurately. The beam element was represented by 3 translational (axial, lead lag, and flap) and 3 corresponding rotational degrees of freedom (DOF) and would generally result in 15 DOFs for each beam element. For an aerodynamics model, a refined aerodynamic model was employed using 16 aerodynamic panels on each blade to capture BVI more accurately, and aerodynamic panels were more densely distributed outboard.

Unsteady lift and moment in the attached flow are calculated based on compressible thin-airfoil theory. Because the steady airloads are obtained from airfoil tables and the lift deficiency effects are usually accounted for in the wake-induced velocity, only the unsteady, noncirculatory effects need to be included for a total airload calculation. The unsteady aerodynamics model selected in the CAMRAD II code was based on the modified ONERA EDLIN theory.[17] The modifications were mainly for less complexity when interfaced with the comprehensive analysis code, such as an exclusion of steady loads calculation, a calculation about the quarter chord for unsteady airloads, or an extension to the reverse flow region. The lift effect produced by the steady, quarter chord upwash was also added as a part of the unsteady airloads calculation.

The rotor vortex filaments are convected from each rotating blades, and the wake is dominated by the blade tip vortices that are trailed from the tips of each rotor blade. The corresponding rotor wake trajectories are described in terms of the blade rotational speed as well as the free stream velocity. The induced velocity is calculated from the Biot–Savart law, by integrating over the complete wake surface,

$$\Delta \boldsymbol{v} = -\int \frac{\Gamma}{4\pi} \cdot \frac{\boldsymbol{r} \times \mathrm{d}\sigma}{|\boldsymbol{r}|^3}$$

where the vector $\boldsymbol{r}$ is at a distance, $\mathrm{d}\boldsymbol{\sigma}$, from the vortex filament to the aerodynamic computation point and Γ is the vortex strength of the trailed filaments.

For the rotor wake structure, the trailed vortices are modeled by two different free-wake approaches in CAMRAD II: a single-trailer wake model and a multiple-trailer wake model. The single-trailer free-wake model includes a rolled-up vortex model that is assumed to be formed at the tip of the blade.[18] The multiple-trailer free-wake model has discrete trailed vortex filaments convected from each of the aerodynamic panel edges. These trailed filaments at the panel edges can be consolidated into a single rolled-up line, using the trailed vorticity moment to scale the rate of rollup.

The basic assumption of the consolidation model is that adjacent trailed vortex lines of the same sign eventually roll up into a single vortex, located at the centroid of the original vorticity distribution. The trailed vorticity is partitioned into sets of adjacent lines that have the same sign. The total strength G, centroid r_C, and moment (radius of gyration) r_G of the trailed vorticity in the set are

$$G = \int -\frac{\partial \Gamma}{\partial r} \cdot \mathrm{d}r, \qquad Gr_C = \int -\frac{\partial \Gamma}{\partial r} \cdot r \, \mathrm{d}r$$

$$Gr_G^2 = \int -\frac{\partial \Gamma}{\partial r} \cdot (r - r_C)^2 \, \mathrm{d}r$$

where Γ is the blade bound circulation. The characteristic time r_G^2/G is taken as a measure of the rate of consolidation. Thus, for trailed vortex elements at wake age τ, the total strength and moment are evaluated at the time $(t - \tau)$ that the vorticity is created and are used to calculate the time constant

$$\tau_{\mathrm{cons}} = k_{\mathrm{cons}} \cdot r_G^2 \big/ G$$

Then the fraction of rollup is

$$f_{\mathrm{cons}} = (\tau - \tau_B)^n \big/ \tau_{\mathrm{cons}}^n$$

The consolidation begins at wake age τ_B. The consolidation can be accomplished by entrainment or by compression. With the entrainment form, vortex lines are consolidated into a single line of strength $f_{\mathrm{cons}} G$. With the compression form, f_{cons} is the fraction of consolidation. For the results presented here, the entrainment form was used, with $k_{\mathrm{cons}} = 1.0$ and $n = 0.33$. Options to evaluate f_{cons} using exponential[19,20] and linear ($n = 1$) functions were also available, but not used here.

Results and Discussion

The HART-I rotor was modeled using the CAMRAD II comprehensive code.[16,17] The rotor is a 40%, Mach-scaled model of the hingeless BO-105 main rotor with a radius of 2 m and a root cutout of 0.35 m, operating at a nominal speed of 1040 rpm. The rotor blade has a standard rectangular tip with a solidity of 0.077. It has a modified NACA 23012 airfoil with a chord length of 0.121 m and −8 deg of linear twist.

Calculations for three test cases, BL (run 140), MN (run 138), and MV (run 133), were made. Figure 1 shows the wake geometry obtained using the multiple-trailer model (entrainment form). Figure 1 shows the wake geometry behind each of the four rotor blades, with the reference blade at 110-deg azimuth. The consolidation distance of the vortex filaments is longer behind the advancing side than behind the retreating blade, which reflects a large value of the consolidation characteristic time r_G^2/Γ on the advancing side. Unlike the single-trailer wake model, it is found that vortex filament bundling in the multiple-trailer vortex model occurs not only near the blade tip but also in the blade midspan. Recall that adjacent trailed vortex lines with the same sign are consolidated into a single rolled-up trailer. Thus, when the loading on the blade is negative, there are three rolled-up trailers in the consolidated wake.

For the trimmed solution, the rotor was trimmed to the thrust and the hub aerodynamic moments (pitching and rolling). The magnitudes of the measured hub moments were small. For the MN and MV cases, the 3-per-revolution pitch control input was added, and then the rotor was retrimmed to reach the trim targets.

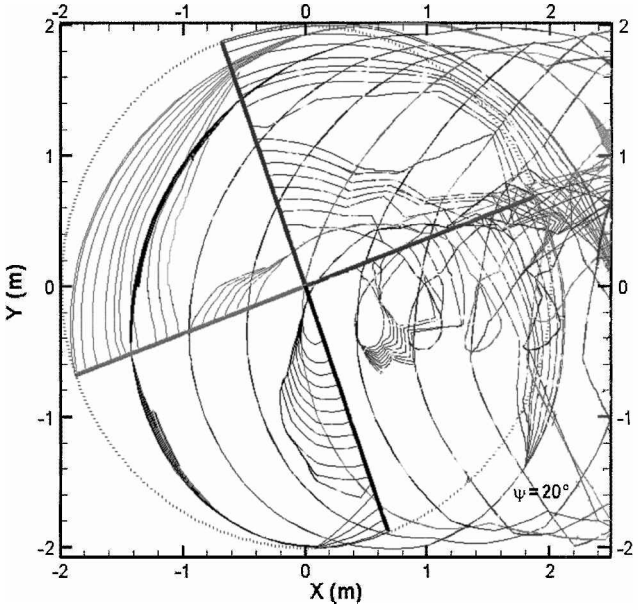

Fig. 1 Multiple-trailer wake geometry convected from each of the rotor blades in the entrainment form (reference blade at 20 deg of azimuth).

Blade Section Airloads

Blade section airloads were obtained by integrating the measured blade surface pressures along the airfoil chord at the fully instrumented radial stations. For the BL case, the measured nondimensional normal forces M^2c_n are shown as functions of azimuth angle in Fig. 2, at the blade span locations of 87 and 97%. The measured data show strong 2-per-revolution variation of lift on the front of the rotor disk and sharp fluctuations of the BVI induced loading on the advancing and retreating sides. Calculated lift distributions using the single-trailer and multiple-trailer free-wake models are plotted with the measured data. The CAMRAD II single-trailer wake model produces poor results for the 2-per-revolution lift distribution. Although the CAMRAD II calculations are slightly better outboard (97%), there is a significant discrepancy in the 2-per-revolution loading. A similar trend was observed in earlier 2GCHAS calculation efforts.[13,14] The multiple-trailer free-wake model, however, shows good lift prediction for both the span locations. These results imply that the discrepancy observed in HART-I airload correlation efforts is caused by the use of single-trailer wake models in the comprehensive codes.

For the MN case, the calculated results are compared with the measured nondimensional normal force in Fig. 3, at the blade span locations of 87 and 97%. The measured data show a much larger third harmonic variation of the lift compared with the baseline case, and in fact, the peak-to-peak magnitude in the minimum noise case is more than doubled from the baseline magnitude. This large increase in the peak-to-peak magnitude presumably is mainly caused by the large 3-per-revolution pitch control input. The calculated lift shows good waveform prediction, but neither wake model was able to match well the peak-to-peak amplitude. The multiple-trailer free-wake model gives a slight improvement of lift correlation, compared with the single-trailer wake model.

For the MV case, shown in Fig. 4, the trends are similar to those found in the MN case. Much larger higher harmonics of lift are

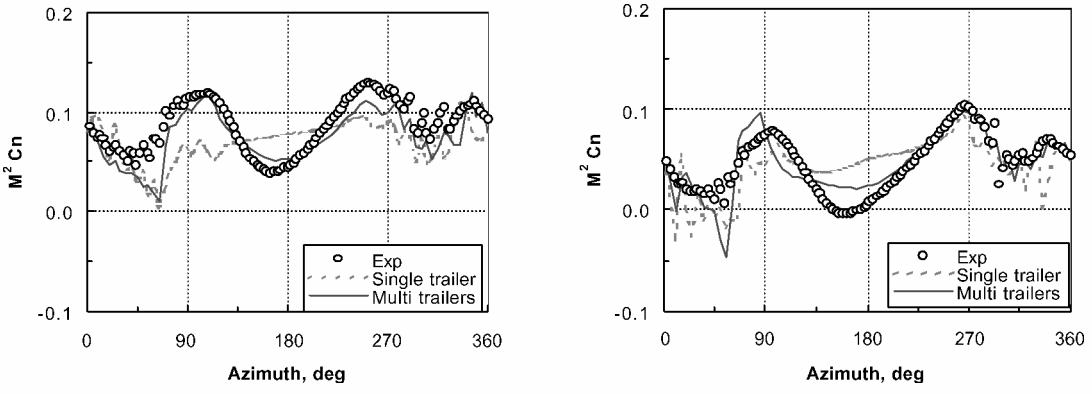

a) HART I, BL, $r/R = 0.87$ **b) HART I, BL, $r/R = 0.97$**

Fig. 2 Calculation of M^2c_n for BL case with single-trailer and multiple-trailer wake models at advance ratio 0.15.

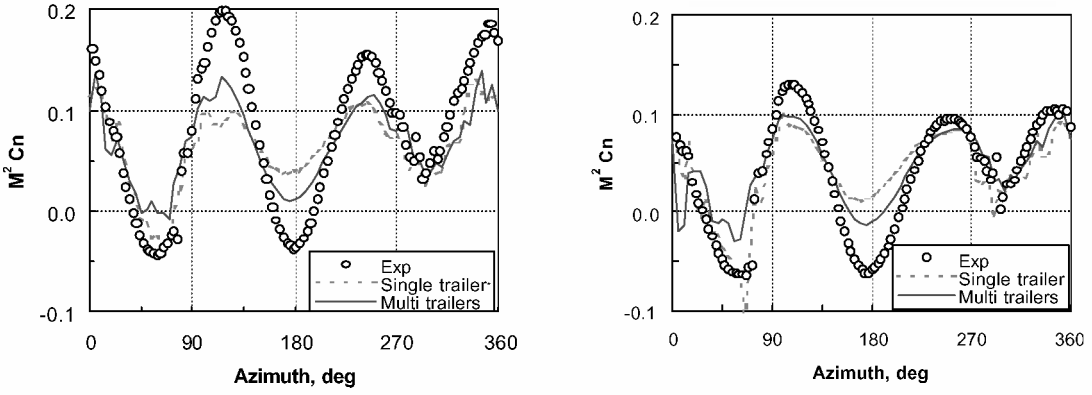

a) HART I, MN, $r/R = 0.87$ **b) HART I, MN, $r/R = 0.97$**

Fig. 3 Calculation of M^2c_n for MN case with single-trailer and multiple-trailer wake models at advance ratio 0.15.

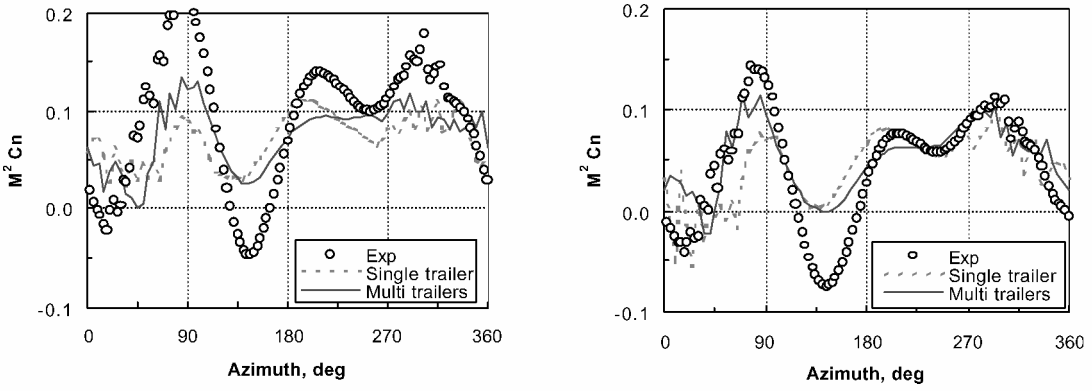

a) HART I, MV, $r/R = 0.87$ **b) HART I, MV, $r/R = 0.97$**

Fig. 4 Calculation of M^2c_n for MV case with single-trailer and multiple-trailer wake models at advance ratio 0.15.

seen in the measured data, and the calculated peak-to-peak magnitude is well below the measured data. This source of the difference between the measured and calculated airloads for the MN and MV is not known.

Blade Deflection

Figure 5a shows correlation of the lead-lag deflection at the blade tip for the three test cases. The CAMRAD II calculations are made utilizing single-trailer and multiple-trailer free-wake models. The waveform of the lead-lag deflection is well predicted for all three cases, but the calculated mean deflection is shifted toward the leading edge by more than one quarter-chord length (1 quarter chord = 3 cm). The two wake models produce essentially the same results for the lag deflection. The difference between measured and calculated mean lag deflection is probably produced by an uncertainty in the blade torque offset or chordwise center-of-gravity position.

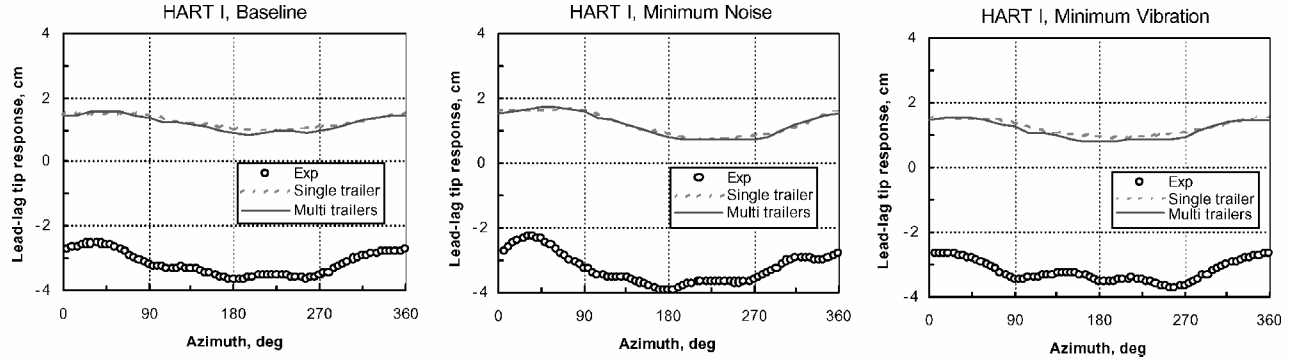

a) Lead-lag deflection at blade tip

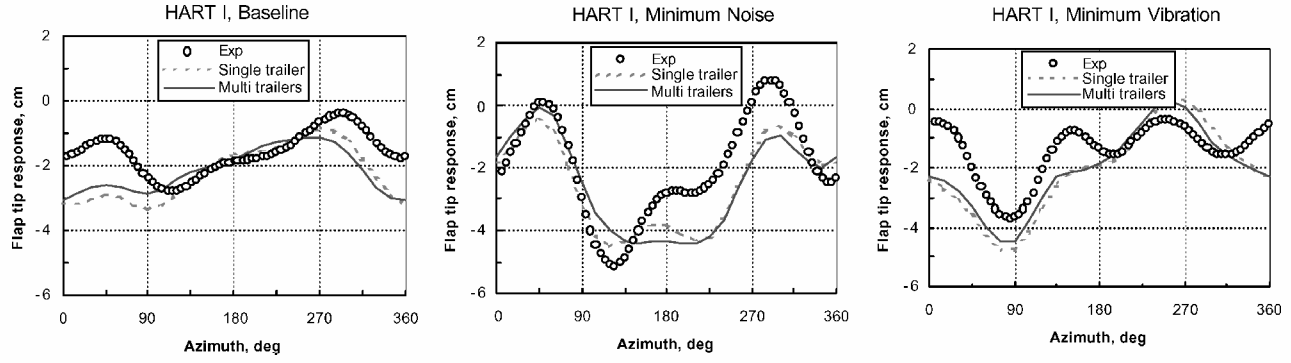

b) Flap deflection at blade tip

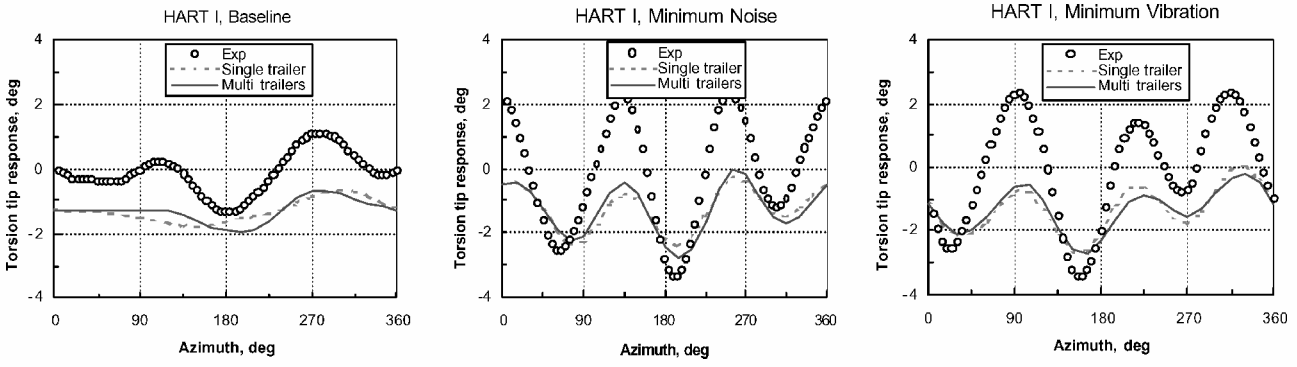

c) Torsion deflection at blade tip (as function of azumuth)

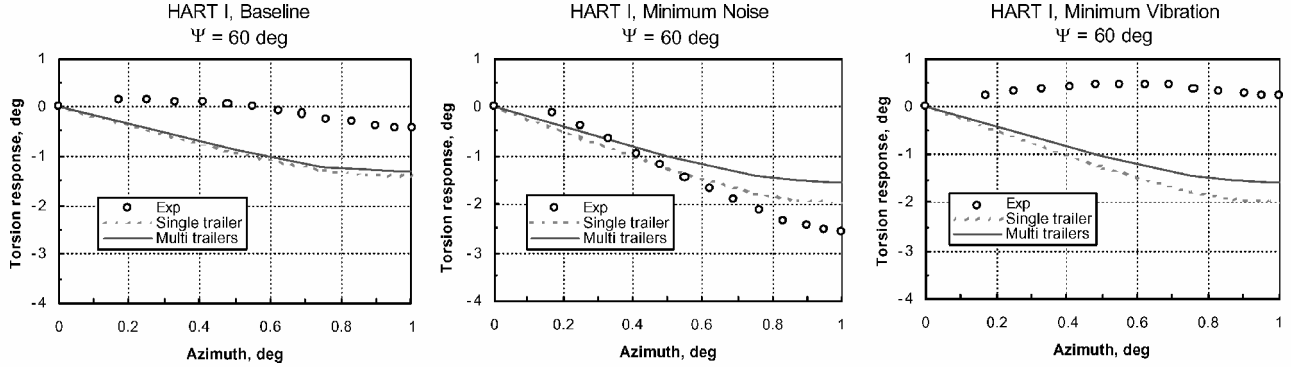

d) Torsion deflection at 60-deg azimuth (as function of blade span)

Fig. 5 Calculated blade response for BL, MN, and MV cases, using single-trailer and multiple-trailer wake models, at an advance ratio of 0.15.

The flap deflection at the blade tip is shown in Fig. 5b for the three cases (BL, MN, and MV). The peak-to-peak amplitude and phase of the flap deflection are well predicted. As observed similarly in prediction for the lag deflection, the two free-wake models produce essentially the same results for the flap deflection.

In earlier studies,[14,15] the elastic torsion was found to be critical to accurate airload prediction, whereas lead-lag and flap deflections were less important. Figures 5c and 5d show the elastic torsion at the blade tip as a function of azimuth angle and blade span, respectively. The calculated mean values of elastic torsion are low for all three (BL, MN, and MV) cases, and also the peak-to-peak magnitudes, are smaller than measured, for both the multiple-trailer and the single-trailer wake models. The spanwise variation of the elastic torsion is almost linear, so that the difference between the measured and calculated elastic torsion at the blade tip is fractionally spread along the span. The azimuthal differences between measured and calculated elastic torsion are consistent with the differences between the section airloads, shown in Fig. 2. The measured torsion deflection exhibits more 2-per-revolution content for the BL case, and more 3-per-revolution content for the MN and MV cases. Because the 3-per-revolution response in the MN and MV cases is caused by the 3-per-revolution pitch input, there probably is some feature of the blade structural dynamics that has not been properly modeled in the calculations, which leads to the underprediction of the torsion and airloads.

Geometry of Wake Tip Vortex

Measurements of selected tip vortex wake segments were reported at the azimuth angles of 35 and 295 deg in Ref. 10. For the BL case, Fig. 6 shows correlation of tip vortex wake geometry in the top

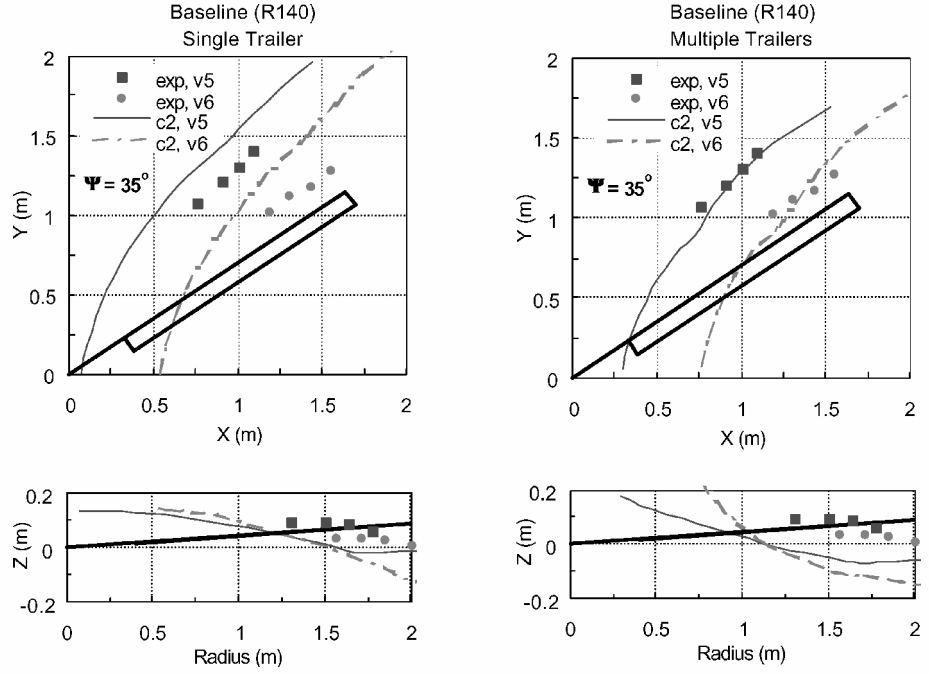

a) Advancing side, Ψ = 35 deg

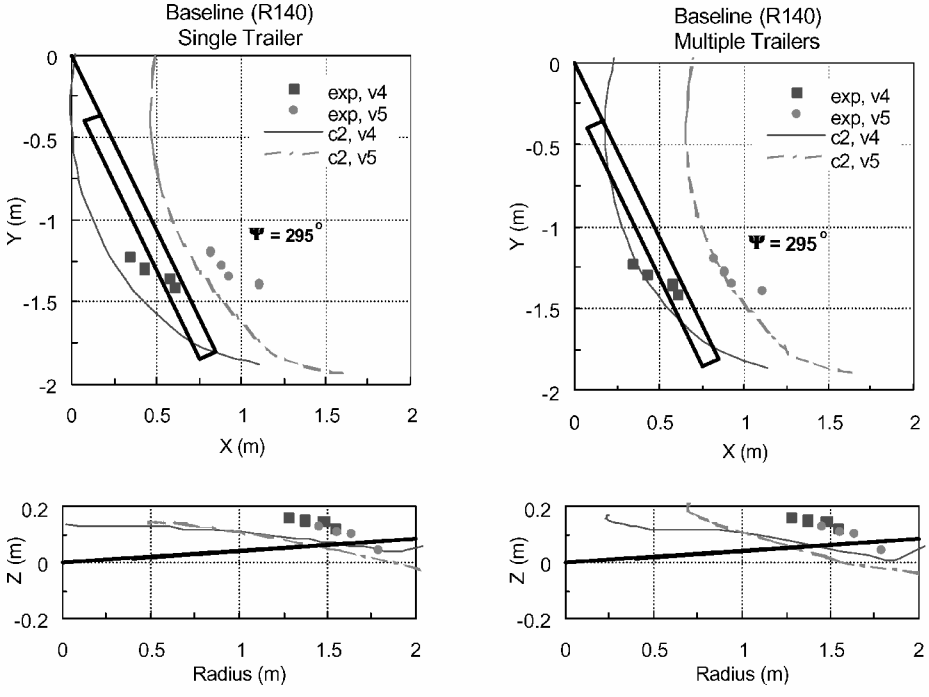

b) Retreating side, Ψ = 295 deg

Fig. 6 Comparison of measured and calculated tip vortex filament locations with single-trailer and multiple-trailer wake models for BL case.

view and side view, using both single-trailer wake and multiple-trailer wake models in CAMRAD II. The top view indicates the location of tip vortices where significant BVIs are considered to occur, and the side view determines the miss distance of the tip vortices. The miss distance is the vertical distance between the passing blade and tip vortices. The fifth and sixth vortex filaments (v5 and v6 in Fig. 6) were understood as near the severe BVI locations and convected downstream from the third and fourth blades, respectively. The single-trailer wake prediction for tip vortex locations in the top view confirms the earlier 2GCHAS study,[13,14] and the calculation consistently lags the measured data by about two chord lengths for an azimuth of 35 deg and somewhat less for an azimuth of 295 deg. The multiple-trailer wake model shows excellent prediction in the top view, unlike the single-trailer wake model.

The miss distance (side view) is shown in Fig. 6 for the BL case. The measured tip vortices cross the reference (passing) blade. The single-trailer wake model predicts the tip vortex locations to be below the blade, hence, below the measurements, and the multiple-trailer model predicts the tip vortex to be even lower. Consequently, the intersections of the blade and tip vortices are predicted to occur more inboard than the measured intersections. Because of the importance of the miss distance to the resulting noise and vibration, as well as to the airloads, it will be important to improve the calculations of miss distance.

For the MN and MV cases, trends similar to the BL case are observed, as shown in Figs. 7 and 8. The multiple-trailer wake model shows good correlation of the tip vortex geometry in the top view, whereas the single-trailer wake model shows a lag of the tip vortex

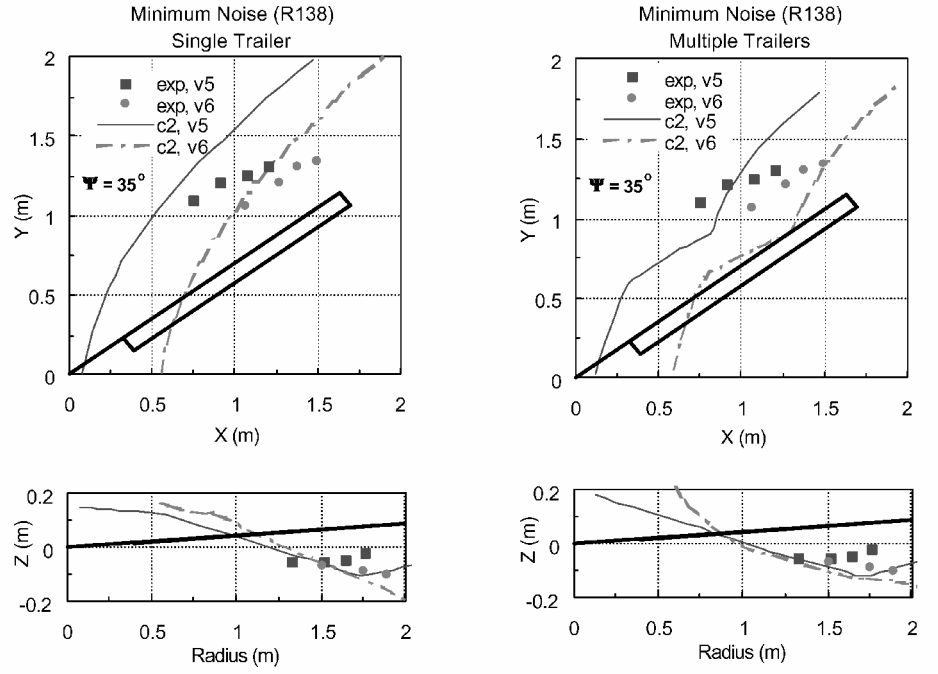

a) Advancing side, Ψ = 35 deg

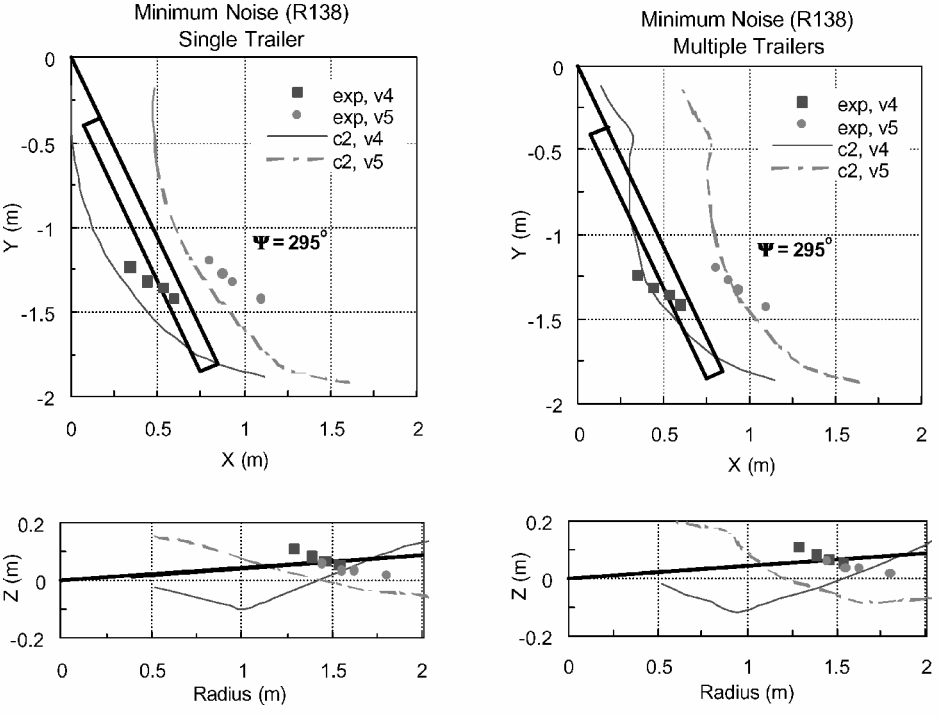

b) Retreating side, Ψ = 295 deg

Fig. 7 Comparison of measured and calculated tip vortex filament locations with single-trailer and multiple-trailer wake models for MN case.

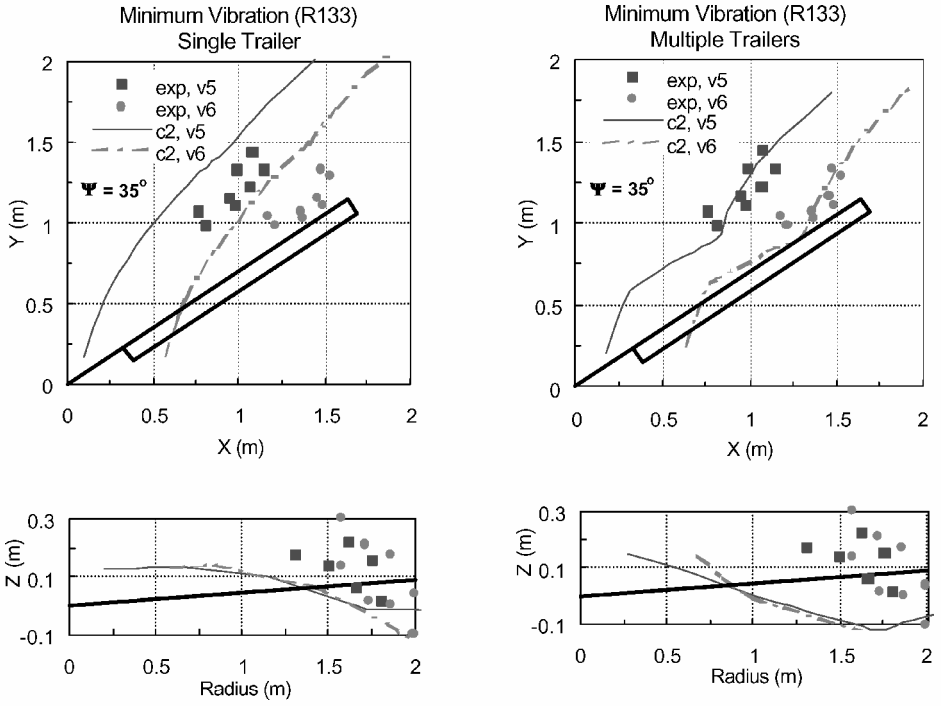

a) Advancing side, Ψ = 35 deg

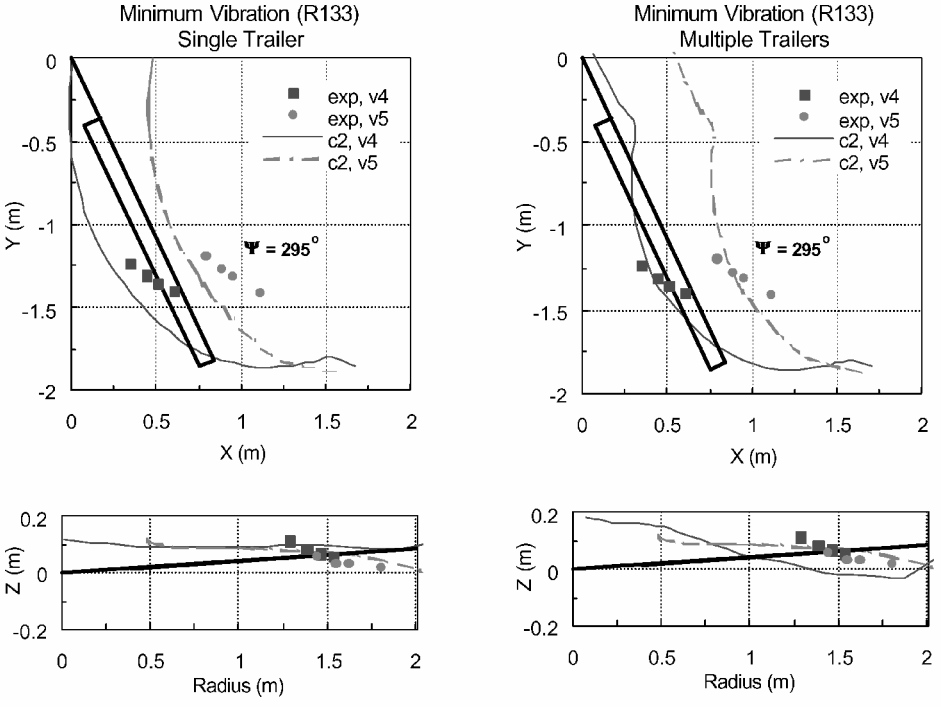

b) Retreating side, Ψ = 295 deg

Fig. 8 Comparison of the measured and calculated tip vortex filament locations with single-trailer and multiple-trailer wake models for MV case.

locations from the measured data. The calculated vertical position is generally below the measured position.

Conclusions

Calculated blade airloads, motion, and wake geometry are compared with measurements from the HART-I rotor. The calculations were performed using the comprehensive analysis CAMRAD II, with single-trailer and multiple-trailer free-wake models.

The multiple-trailer wake model produces significantly better airloads correlation than the single-trailer wake model. It gives good correlation for the airloads in the BL case. In particular, the 2-per-revolution normal force is well predicted, which was not possible in previous investigations using the single-trailer wake model. The multiple-trailer wake model also showed good correlation of the measured and calculated wake geometry in the top view, whereas the single-trailer wake model gives positions of the wake geometry well forward of the measured positions.

However, not all of the calculations were improved with the multiple-trailer wake model. The measured airloads in the minimum noise and minimum vibration cases exhibit larger 3-per-revolution content than the calculated airloads. The measured and calculated blade tip torsion motion show differences in 2- and 3-per-revolution content that are consistent with the differences in the airloads.

The miss distance predictions are deteriorated with the multiple-trailer wake model compared with the single-trailer wake model for all BL, MN, and MV cases. Even with some poorly predicted

parameters, it is obvious that a multiple-trailer wake model significantly improves the understanding of the source of discrepancy from the previous HART-I correlation efforts. Generally the calculated tip vortex positions are below the measured positions.

Acknowledgments

The authors would like to thank Chee Tung at the U.S. Army Aeroflightdynamics Directorate for his invaluable technical advice and encouragement. Furthermore, the authors appreciate the higher-harmonic-control aeroacoustic rotor test (HART) team for providing the HART-I test data.

References

[1]Splettstoesser, W. R., Schultz, K. J., Kube, R., Brooks, T. F., Booth, E. R., Niesel, G., and Streby, O., "BVI Impulsive Noise Reduction by Higher Harmonic Pitch Control: Results of a Scaled Model Rotor Experiment in the DNW," *Proceedings of the 17th European Rotorcraft Forum*, German Society for Aeronautics and Astronautics, Bonn, Federal Republic of Germany, Sept. 1991, pp. 91–61.

[2]Brooks, T. F., Booth, E. R., Jolly, J. R., Yeager, W. T., and Wilbur, M. L., "Reduction of Blade-Vortex Interaction Noise Through Higher Harmonic Pitch Control," *Journal of the American Helicopter Society*, Vol. 35, No. 1, 1990, pp. 86–91.

[3]Polychroniadis, M., "Generalized Higher Harmonic Control—Ten Years of Aerospatiale Experience," *Proceedings of the 16th European Rotorcraft Forum*, The Royal Aeronautical Society, London, U.K., Sept. 1990.

[4]Brooks, T. F., Booth, E., Boyd, D. D., Splettstoesser, W. R., Schultz, K. J., Kube, R., Niesl, G. H., and Streby, O., "HHC Study in the DNW to Reduce BVI Noise—an Analysis," *Proceedings of the American Helicopter Society/Royal Aeronautical Society International Technical Specialists' Meeting—Rotorcraft Acoustics and Fluid Dynamics*, American Helicopter Society, Alexandria, VA, Oct. 1991.

[5]Splettstoesser, W. R., Niesl, G., Cenedese, F., Nitti, F., and Papanikas, D. G., "Experimental Results of the European HELINOISE Aeroacoustic Rotor Test in the DNW," *Proceedings of the 19th European Rotorcraft Forum*, Agusta Aerospace Corp., Verese, Italy, Sept. 1993.

[6]Yu, Y. H., Gmelin, B., Heller, H., Philippe, J. J., Mercker, E., and Preisser, J. S., "HHC Aeroacoustics Rotor Test at the DNW—the Joint German/French/US HART Project," *Proceedings of the 20th European Rotorcraft Forum*, National Aerospace Lab., Amsterdam, The Netherlands, Sept. 1994.

[7]Gmelin, B. L., Heller, H. H., Mercker, E., Philippe, J. J., Preisser, J. S., and Yu, Y. H., "The HART Program, a Quadrilateral Cooperative Research Effort," *Proceedings of the 51st Annual Forum of American Helicopter Society*, American Helicopter Society, Alexandria, VA, May 1995, pp. 695–709.

[8]Splettstoesser, W. R., Kube, R., Wagner, W., Seelhorst, U., Boutier, A., Micheli, F., Mercker, E., and Pengel, K., "Key Results from a Higher Harmonic Control Aeroacoustic Rotor Test (HART)," *Journal of the American Helicopter Society*, Vol. 42, No. 1, 1997, pp. 58–78.

[9]Beaumier, P., Demargne, A., Prieur, J., Rahier, G., Spiegel, P., Kube, R., van der Wall, B. G., Schultz, K. J., Splettstoesser, W., Tung, C., Gallman, J., Yu, Y. H., Brooks, T. F., Burley, C. L., and Boyd, D. D., "Aerodynamic and Acoustic Effects of Higher Harmonic Control on Helicopter Rotor Blade–Vortex Interaction: Predictions and Preliminary Validation," 75th AGARD Fluid Dynamics Panel Symposium on Aerodynamics and Acoustics of Rotorcraft, Oct. 1994.

[10]Tung, C., Gallman, J. M., Kube, R., Wagner, W., van der Wall, B., Brooks, T. F., Burley, C. L., Boyd, D. D., Rahier, G., and Beaumier, P., "Prediction and Measurement of Blade–Vortex Interaction Loading," *Proceedings of the 1st Joint Confederation of European Aerospace Studies/AIAA Aeroacoustics Conference*, DLR Programme Directorate Aeronautics, Braunschweig, Germany, June 1995.

[11]Kube, R., Splettstoesser, W. R., Wagner, W., Seelhorst, U., Yu, Y. H., Tung, C., Beaumier, P., Prieur, J., Rahier, G., Spiegel, P., Boutier, A., Brooks, T. F., Burley, C. L., Boyd, D. D., Mercker, E., and Pengel, K., "HHC Aeroacoustic Rotor Tests in the German Dutch Wind Tunnel: Improving Physical Understanding and Prediction Codes," *Proceedings of the 52nd Annual Forum of American Helicopter Society*, American Helicopter Society, Alexandria, VA, May 1996.

[12]Rahier, G., and Delrieux, Y., "Blade–Vortex Interaction Noise Prediction Using a Rotor Wake Rollup Model," *Journal of Aircraft*, Vol. 34, No. 4, 1997, pp. 522–530.

[13]Lim, J. W., and Tung, C., "2GCHAS Prediction of HART Blade–Vortex Interaction Loading," *Proceedings of the American Helicopter Society Technical Specialists' Meeting for Rotorcraft Acoustics and Aerodynamics*, American Helicopter Society, Alexandria, VA, Oct. 1997.

[14]Lim, J. W., Tung, C., and Yu, Y. H., "Prediction of Blade–Vortex Interaction Airloads with Higher-Harmonic Pitch Controls Using the 2GCHAS Comprehensive Code," *Journal of Pressure Vessel Technology*, Vol. 123, No. 4, 2001, pp. 469–474.

[15]Wachspress, D. A., and Quackenbush, T. R., "Wake Model Requirements for Prediction of BVI Airloads," *Proceedings of the American Helicopter Society Technical Specialists' Meeting for Rotorcraft Acoustics and Aerodynamics*, American Helicopter Society, Alexandria, VA, Oct. 1997.

[16]Johnson, W., "Rotorcraft Aerodynamics Models for a Comprehensive Analysis," *Proceedings of the 54th Annual Forum of American Helicopter Society*, American Helicopter Society, Alexandria, VA, May 1998, pp. 71–94.

[17]Johnson, W., CAMRAD II: Volume II Components Theory, Release 4.2, Johnson Aeronautics, Palo Alto, CA, 2003.

[18]Scully, M. P., "Computation of Helicopter Rotor Wake Geometry and its Influence on Rotor Harmonic Airloads," Aeroelastic and Structures Research Lab., Dept. of Aeronautics and Astronautics, Massachusetts Inst. of Technology, ASRL TR 178-1, Cambridge, MA, March 1975.

[19]Yeo, H. S., and Shinoda, P. M., "Investigation of Rotor Loads and Vibration at Transition Speed," *Proceedings of the 58th Annual Forum of American Helicopter Society*, American Helicopter Society, Alexandria, VA, June 2002.

[20]Johnson, W., "Influence of Wake Models on Calculated Tiltrotor Aerodynamics," *Proceedings of the American Helicopter Society Technical Specialists' Meeting for Aerodynamics, Acoustics, and Testing and Evaluation*, American Helicopter Society, Alexandria, VA, Jan. 2002.